materials

MDPI

Communication

Energy Storage Characteristics of $BiFeO_3/BaTiO_3$ Bi-Layers Integrated on Si

Menglin Liu [1], Hanfei Zhu [1], Yunxiang Zhang [1], Caihong Xue [1] and Jun Ouyang [1,2,3,*]

1 Key Laboratory for Liquid−Solid Structural Evolution and Processing of Materials (Ministry of Education), School of Materials Science and Engineering, Shandong University, Jinan 250061, China; liumenglinnadou@163.com (M.L.); hfzhu1986@163.com (H.Z.); zhangyunxiangls@163.com (Y.Z.); chxueaj@163.com (C.X.)

2 Suzhou Institute of Shandong University, Suzhou 215123, China

3 National Institute of Standards and Technology, Gaithersburg, MD 20899, USA

* Correspondence: ouyangjun@sdu.edu.cn; Tel.: +86-531-8839-5816; Fax: +86-531-8839-2439

Academic Editor: Yuhang Ren

Received: 29 September 2016; Accepted: 11 November 2016; Published: 18 November 2016

Abstract: $BiFeO_3/BaTiO_3$ bi-layer thick films (~1 μm) were deposited on $Pt/Ti/SiO_2/(100)$ Si substrates with $LaNiO_3$ buffer layers at 500 °C via a rf magnetron sputtering process. X-ray diffraction (XRD) analysis revealed that both $BiFeO_3$ and $BaTiO_3$ layers have a (00*l*) preferred orientation. The films showed a small remnant polarization (P_r ~ 7.8 μC/cm^2) and a large saturated polarization (Ps ~ 65 μC/cm^2), resulting in a slim polarization-electric field (*P-E*) hysteresis loop with improved energy storage characteristics (W_c = 71 J/cm^3, η = 61%). The successful "slim-down" of the *P-E* loop from that of the pure $BiFeO_3$ film can be attributed to the competing effects of space charges and the interlayer charge coupling on charge transport of the bi-layer film. The accompanying electrical properties of the bi-layer films were measured and the results confirmed their good quality.

Keywords: ferroelectrics; lead-free; energy storage; bilayer; $BiFeO_3$; $BaTiO_3$; Si

1. Introduction

Densities of electrical energy stored in or released from a dielectric can be calculated from their characteristic dielectric displacement-electric field (*D-E*) curves by the formula [1]:

$$W_c = \int_0^{D_s} EdD, W_d = \int_{D_r}^{D_s} EdD \tag{1a}$$

$$\eta = \frac{W_d}{W_c}, \tag{1b}$$

where W_c is the charged (stored) energy density, W_d is the discharged (released) energy density and η the energy efficiency. D_s and D_r are the saturated/maximum and remnant electrical displacements, respectively. For an ideal linear dielectric with a relative dielectric constant ε_r, $D = \varepsilon_0\varepsilon_r E$ and $D_r = 0$, the energy densities are given by [1]:

$$W_c = \frac{1}{2}\varepsilon_0\varepsilon_r E_{\max}^2, \tag{2a}$$

$$W_d = W_c = \frac{1}{2}\varepsilon_0\varepsilon_r E_{\max}^2, \tag{2b}$$

and the efficiency η equals 1. Here ε_0 is the vacuum dielectric constant, E_{max} is the maximum applicable electric field which increases with the breakdown field E_b ($E_{max} \approx E_b$ for an ideal dielectric). On the other hand, non-linear dielectrics like ferroelectrics usually don't have $D \propto E$ or $D_r = 0$, hence $W_c > W_d$

and $\eta < 1$. Nevertheless, Equation (2a) can still be used for the estimation of energy densities W_c in non-linear dielectrics, wherein ε_r is the average or effective dielectric constant.

To meet the demands in developing portable and integrable power electronics, thin film ceramic capacitors with a high energy storage density W_c and a high efficiency η have been intensively investigated [2–4]. The previous studies on thin film ceramic capacitors have been focused on lead-containing perovskite ferroelectrics, including BNZ-PT, BNT-PT and BNH-PT [5–7]. *P-E* (*) curve of a typical ferroelectric is presented in Figure 1. In this figure, the green area represents the discharged energy density (W_d), the yellow area encircled by the hysteresis loop is the energy loss (W_{loss}), and the charged energy density is the sum of the two, $W_c = W_d + W_{\text{loss}}$. It's obvious that the energy storage characteristics of a ferroelectric strongly depend on the shape of its *P-E* loop.

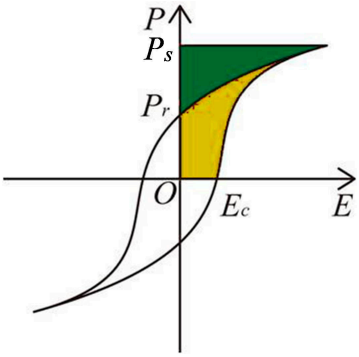

Figure 1. Schematic of a ferroelectric *P-E* loop. The green area is the discharged energy density W_d, while the yellow area is the energy loss of one charge-discharge cycle (W_{loss}).

In the past decade, large energy storage densities (40 J/cm^3–60 J/cm^3) have been reported in lead-containing ferroelectric films together with good energy efficiencies (40%–60%) [6–9]. However, the growing environment concerns on lead and the usually complex compositions of the solid solutions being used are the two major drawbacks of the lead-containing ferroelectric capacitors. In order to minimize the environmental impact and promote a manufacturing-friendly preparation process, single component lead-free perovskites have been investigated by several research groups for applications in thin film dielectric capacitors [10–14]. Among them, $BiFeO_3$ and $BaTiO_3$ films are most popular candidates [13,14]. The former has a giant saturated polarization and tunable electrical properties via strain or chemical doping, while the latter has excellent dielectric properties (large ε_r and high E_b) and hence has been broadly used in multi-layer ceramic capacitors (MLCC). However, large leakage currents and poor energy efficiencies associated with $BiFeO_3$ thin films have hindered its further development for energy storage applications. On the other hand, a small saturated polarization of $BaTiO_3$ has capped its energy densities (see Equation (1a)) and limited most of its capacitor applications in MLCC.

According to Equation 1, dielectrics with high E_b and ε_r, a small remnant polarization and a large saturated polarization are ideal for high efficiency energy-storage applications. In this work, we demonstrate a novel approach to compensate for the lack of a single material with the above properties. We prepared ferroelectric bilayers of $BiFeO_3/BaTiO_3$ on Si substrates via an in-situ rf magnetron sputtering process at 500 °C. Textured growth of the bi-layer films at this moderate temperature was promoted by using a $LaNiO_3$ template layer. The resulted thin film capacitors of $Au/BiFeO_3/BaTiO_3/LaNiO_3/Pt/Ti$ not only showed good dielectric properties (high ε_r and low leakage current), but also a slim *P-E* hysteresis featuring an enhanced energy storage density and efficiency, as compared with those of single layers of $BiFeO_3$ and $BaTiO_3$ on Si. The improved energy storage characteristics are interpreted based on our understanding of the charge transport process, which is dominated by the effect of space charges at low electric fields and by the interface charge coupling at high electric fields.

2. Experimental Section

$BiFeO_3/BaTiO_3$ bi-layer thick films were fabricated on $Pt/Ti/SiO_2/(100)Si$ substrates buffered with a $LaNiO_3$ layer via a rf magnetron sputtering process. Commercially available ceramic targets of $BaTiO_3$, $Bi_{1.05}FeO_3$ and $LaNiO_3$ (4N purity, Φ = 50 mm, L = 5 mm) were used in the deposition process, which was carried out in a multi-target magnetron sputtering system with a base pressure of 2.0×10^{-4} Pa. Firstly, a 120-nm-thick Pt/Ti layer was deposited as the bottom electrode at 300 °C in a pure argon atmosphere. Then the $LaNiO_3$, $BaTiO_3$ and $BiFeO_3$ layers were sequentially sputtered at 500 °C in a mixed gas of Ar and O_2. The thickness of the $BiFeO_3/BaTiO_3$ bi-layer was about 1 μm with a 1:1 thickness ratio. Lastly, the as-deposited multi-layer thick film was cooled down at a rate of 6 °C/min–8 °C/min in pure oxygen. The deposition parameters of the sputtering process were summarized in Table 1 and the schematics of experimental procedures was shown in Figure 2. For electrical characterizations, circular Au top electrodes with a diameter of 200 μm were deposited at room temperature by using a shadow mask.

Table 1. Deposition Parameters of the Sputtering Process for $BiFeO_3/BaTiO_3$ Bi-layer Films on $SiO_2/(100)$ Si Substrates.

Sputtering Parameters	BFO	BTO	LNO
Sputtering power (W)		100	
Substrate temperature (°C)		500	
Sputtering pressure (Pa)	1.2		0.3
Sputtering atmosphere	Ar + O_2 (4:1 flow ratio)		
Cooling atmosphere and pressure	Pure oxygen, 2.5 Pa		
Pt/Ti sputtering parameters	300 °C, 0.3 Pa, 55 W, pure Ar		

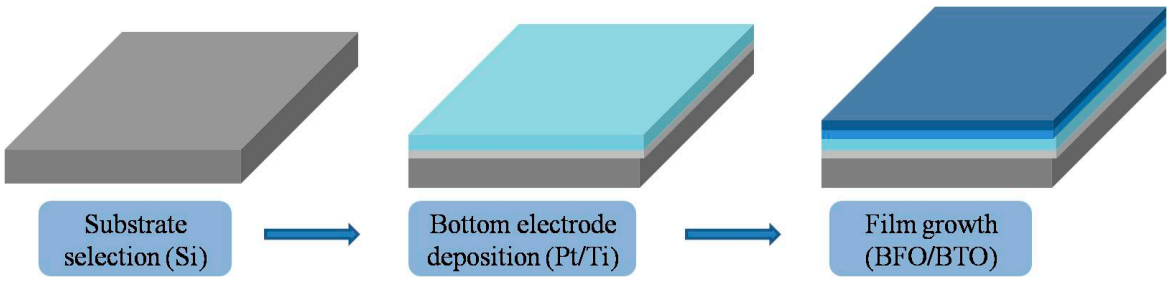

Figure 2. Schematics of the experimental procedures.

The phase structures and crystallographic orientations of the bilayer films were characterized by using X-ray diffraction (XRD) θ-2θ scans with a Ni-filtered Cu-Kα radiation resource (Dmax-rc, Monaghan, Ireland) and pole figures (R-156 Axis Spider, SmartLab® Rigaku, Tokyo, Japan, 40 kV, 200 mA). A commercially available MicroNano D-5A Scanning Probe Microscope (SPM) (MicroNano, Shanghai, China) was used to analyze the surface morphology while the cross-sectional thin film morphology was analyzed by using a thermal field emission scanning electron microscope (SEM) (SU-70, HITACHI, Hitachi, Japan) The room temperature ferroelectric hysteresis loops (P-V) and leakage currents (I-V) were measured by using a Radiant Precision Premium II ferroelectric tester (Radiant Technology, Albuquerque, NM, USA). The dielectric properties were measured by using a high precision digital bridge (QuadTech 7600 Plus Precision LCR Meter, IET LABS, Inc., West Roxbury, MA, USA).

3. Results

3.1. Microstructures and Crystallographic Orientations

Figure 3a shows the XRD 2θ scan spectrum of the $BiFeO_3/BaTiO_3$ bilayer film grown on $LaNiO_3/Pt/Ti/SiO_2/(100)$ Si, which is dominated by the preferred (00*l*) diffraction peaks of the bulk perovskite structures and does not show any crystalline impurities or secondary phases. A tiny amount of (110)-oriented $BaTiO_3$ grains and (100)-oriented tetragonal $BiFeO_3$ grains were detected, which can be attributed to the moderate growth temperature and the effect of residual stress [15,16]. In our previous work [17], it was revealed that a highly (00*l*)-oriented $BaTiO_3$ thin film can be grown on $Pt/Ti/SiO_2/(100)$ Si substrate by using a $LaNiO_3$ buffer layer at 500 °C. Here it is confirmed that the presence of a (*l*00)-oriented $LaNiO_3$ buffer layer promoted the growth of a (00*l*) oriented $BiFeO_3/BaTiO_3$ bi-layer film.

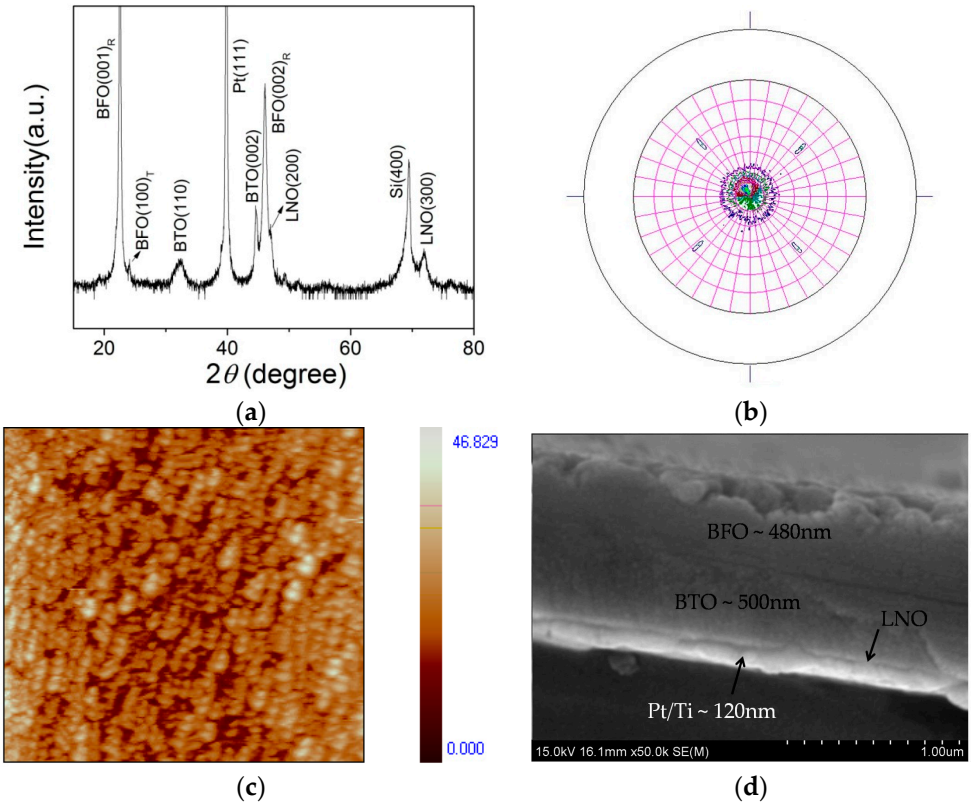

Figure 3. (**a**) XRD 2θ scan spectrum (R-rhombohedral, T- tetragonal for BFO peaks, while the BTO phase is tetragonal); (**b**) X-ray pole figure analyses by using the $(001)_R$ BFO peak; (**c**) AFM surface scan image (5 μm × 5 μm); and (**d**) cross-sectional SEM image of the $BiFeO_3/BaTiO_3$ bi-layer film deposited on $LaNiO_3/Pt/Ti/SiO_2/(100)$ Si substrate.

To further investigate the crystallographic characteristics of the bi-layer film, pole figure analysis was carried out on the {001} $BiFeO_3$ reflection (2θ = 22.56°). During collection of the XRD signals, the sample was rotated by varying the tilt angle ($0° < \psi < 70°$) and the azimuthal angle ($0° < \varphi < 360°$) with respect to the scattering vector. The pole figure of $(001)_{BFO}$, as shown in Figure 3b, revealed a strong diffraction peak at the center (tilt angle $\psi = 0°$), and a set of 4-fold diffraction peaks at $\psi \approx 46°$, corresponding to the {101} $BiFeO_3$ plane. This result confirmed the preferred (00*l*) orientation of the $BiFeO_3$ layer, as suggested by the result of the XRD 2θ scans.

Surface morphology of the $BiFeO_3/BaTiO_3$ bi-layer film is displayed in Figure 3c. It can be seen that the grains of the top $BiFeO_3$ layer are densely packed with an average size of ~200–300 nm.

The surface roughness Ra was measured to be ~4.1 nm, which shows a significant reduction as compared with those of the single layer $BiFeO_3$ films (Ra is on the order of ~10 nm or above) [18–21]. The dense and smooth growth of the $BiFeO_3$ layer can be attributed to the good quality perovskite underlayers of $LaNiO_3/BaTiO_3$. In Figure 3d, the cross-sectional SEM image shows clean and sharp interfaces in the multi-layer thin film. The $BiFeO_3$ and $BaTiO_3$ layers were measured to be ~480 nm and ~500 nm, respectively.

3.2. Energy Storage Characteristics from the P-E Hysteresis Loop

The poling and depoling process of a dielectric under an external electric field simulates the charge-discharge process of a capacitor. Therefore, from the polarization–electric field (*P-E*) hysteresis loop, the energy storage density W_c and the energy efficiency η of the $Au/BiFeO_3/BaTiO_3/LaNiO_3/Pt/Ti$ capacitors can be calculated by using Equation (1). Figure 4a displays the *P-E* hysteresis loop measured at a pseudo-static frequency of 1 kHz for the bi-layer film (under an applied electric field of 1940 kV/cm). A large maximum polarization (P_m ~ 65 μC/cm^2) and a small remnant polarization (P_r ~ 7.8 μC/cm^2) are simultaneously obtained, together with a reduced coercive field E_c (E_c ~ 152 kV/cm) as compared with that of pure $BiFeO_3$ film [22]. These features of the *P-E* curve ensure excellent energy storage characteristics of the film. When compared with pure $BaTiO_3$ films deposited under similar conditions [23], the energy storage density W_c of the bi-layer film reached 71 J/cm^3 (E_{max} = 1940 kV/cm), a 100%–110% improvement, while the energy efficiency η stayed about the same level (~61% vs. 60%–70%). This improvement in W_c can be attributed to a much improved maximum polarization and a high dielectric strength in par with that of a pure $BaTiO_3$ film.

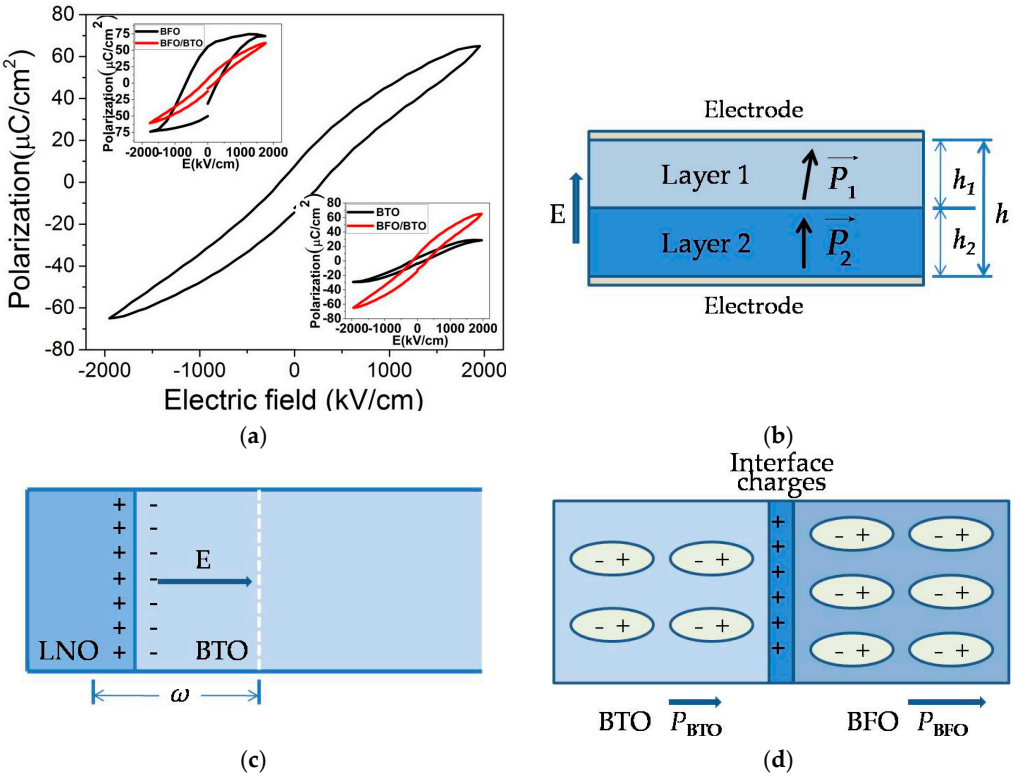

Figure 4. (**a**) Room temperature ferroelectric hysteresis loop of the $BiFeO_3/BaTiO_3$ bi-layer film deposited on $LaNiO_3/Pt/Ti/SiO_2/(100)Si$ substrate, the insets compare *P-E* loops of the pure $BiFeO_3$ and $BaTiO_3$ films with those of the bi-layer film measured under the same electric field [22,23]; (**b**) schematics of the ferroelectric bi-layer considered in our work; (**c**) the space charge effect dominant at a low electric field, ω is the depletion layer width under an electric field E; (**d**) strong interlayer charge coupling dominant at a high electric field (after the $BaTiO_3$ layer has been fully depleted).

The "slim-down"of the *P-E* loop can be explained by the competition between the space charge effect and interlayer charge coupling in the bi-layer film. As demonstrated in our previous study, a space charge layer in $BaTiO_3$ near its interface with $LaNiO_3$ dominates the film's electrical characteristics at a low electric field [24]. Basically, a depletion region with width ω forms at the $BaTiO_3/LaNiO_3$ interface upon the application of a small electric field. The width ω can be computed by [24]:

$$w = \sqrt{\frac{2\varepsilon(V + V_{bi}^*)}{qN_{eff}}}, \quad (3)$$

where V_{bi}^* is the modified built-in voltage, ε is the dielectric constant ($\varepsilon = \varepsilon_0\varepsilon_r$), N_{eff} is the space charge concentration, V is the applied electric voltage and q the electronic charge. The voltage V is concentrated across the depletion region and drives its expansion until the $BaTiO_3$ layer has been fully depleted. It has been shown that the existence and evolution of a depletion layer in a ferroelectric film will cause shrinking and tilting of its *P-E* loop, leading to reduced P_r and E_c [25]. On the other hand, after the $BaTiO_3$ layer has been completely depleted, a substantial amount of bound charges appear at the $BiFeO_3/BaTiO_3$ interface owing to the large difference in polarizations between the two layers. Hence the charge transport of the bi-layer film under a high electric field will be dominated by the interface charge coupling, which can be described by an added energy term $\frac{1}{2\varepsilon_0}\alpha(1-\alpha)(\vec{P_1} - \vec{P_2})^2$ in the Landau-Ginzburg-Devonshire (LGD) thermodynamic potential (free energy density F) of the bilayer thick film [26]:

$$\mathrm{F} = (1-\alpha)\left[\mathrm{F}_1(\vec{P_1}) - \vec{E}\cdot\vec{P_1}\right] + \alpha\left[\mathrm{F}_2(\vec{P_2}) - \vec{E}\cdot\vec{P_2}\right] + \frac{1}{2\varepsilon_0}\alpha(1-\alpha)(\vec{P_1} - \vec{P_2})^2 \quad (4)$$

here $\alpha = h_2/h$ ($h = h_1 + h_2$) is the relative thickness of the second layer, F_i, $\vec{P_i}$ (i = 1, 2) are the bulk free energy density and polarization of the ith layer, and $\vec{E}$ is the applied electric field (see Figure 4b). The third term of the free energy density with the coefficient $\alpha(1-\alpha)$ expresses the energy of electrostatic interaction between the two layers, and it becomes dominant when the field is large enough to allow both layers become fully poled. In this case, the difference between the two polarizations diminishes and the film shows an "average" polarization. In our case, the polarization of the fully poled bi-layer film P_{bi} is close to that of $BiFeO_3$ due to the fact that $P_{BFO} >> P_{BTO}$. The computed P_{bi} by solving the equilibrium state of Equation (4) is close to 50 $\mu C/cm^2$ [21], fairly consistent with the observed P_m value if the linear contribution from dielectric susceptibility to the total polarization is deducted. Therefore, the enhanced energy storage capability of the $BiFeO_3/BaTiO_3$ bi-layer film can be attributed to a combination of space charge effect (dominant at low field, leading to small P_r and E_c) and effect of interlayer charge coupling (dominant at high field, leading to a large P_m).

Figure 5 a shows the leakage current density versus electric field (*J-E*) curve. At an electric field of 100 kV/cm (bias voltage of 10 V), the leakage current density of the bi-layer film is 5.0×10^{-6} A/cm^2. This is about an order of magnitude lower than those reported for single layer $BiFeO_3$ films grown on Si substrates [27,28]. The reduction in leakage current is in good agreement with the observed morphology change shown in AFM and SEM images, i.e., a densely and smoothly grown $BiFeO_3$ film was endowed with a much improved electrical resistivity [29]. In addition, an interface energy barrier φ_B between the $BiFeO_3$ (work function W ~ 4.7 eV) and $BaTiO_3$ (W ~ 4.0 eV) layers can also reduce the leakage current and hence allow the film to be exposed to a large electric field [30,31]. As a result, a high energy density is achieved in the $BiFeO_3/BaTiO_3$ bi-layer film.

Figure 5b displays frequency-dependent relative dielectric constant ε_r and loss tangent tanδ of the bi-layer film. It can be seen that the pseudo static ε_r is about 425 (@1 kHz), which is about 33% and 70% higher than those of the single layer $BaTiO_3$ and BFO films grown on Si, respectively (ε_r ~ 320 for BTO, ε_r ~ 250 for BFO) [22,32]. When the frequency increases from 1 kHz to 1 MHz, ε_r decreases from ~425 to ~380. On the other hand, tan δ varies between 2.4% and 8.4% in the same frequency range,

similar to that of pure BTO films grown on Si. The enhanced dielectric constant ε_r contributes to the improved maximum polarization P_m, based on the relation $P_m = D_m = P + \varepsilon_r \times E_{max}$, where P is the self-polarization and $P \approx P_r$ for ferroelectrics.

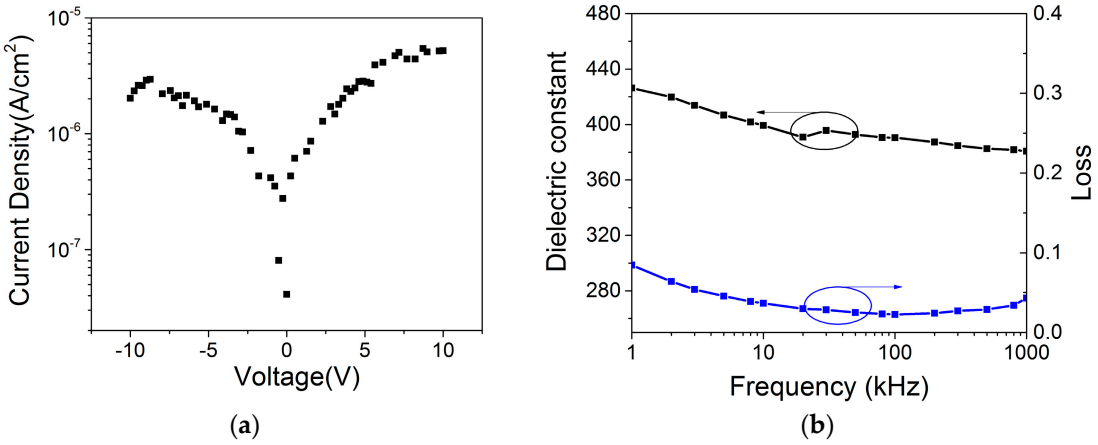

Figure 5. (**a**) Leakage current density vs. voltage (*J-V*) curve; and (**b**) frequency dependent dielectric properties of the $BiFeO_3/BaTiO_3$ bi-layer film.

4. Conclusions

In this study, $BiFeO_3/BaTiO_3$ bi-layer thick films deposited on the $LaNiO_3$ -buffered $Pt/Ti/SiO_2/(100)$ Si substrates display an enhanced energy density and charge-discharge efficiency (W_c = 71 J/cm^3, η = 61%) as compared with those of the single layer films. This enhancement can be attributed to combined effects of space charges and the interlayer charge coupling. The bi-layer film exhibits a low leakage current density (5.0×10^{-6} A/cm^2 at 100 kV/cm) as a result of the dense and smooth film morphology achieved in the BFO layer, which is induced by the high quality underlayer of $BaTiO_3/LaNiO_3$. The relative dielectric constant ε_r is about 33% higher than that of the pure $BaTiO_3$ film and 70% higher than that of the pure BFO film. In conclusion, the $BiFeO_3/BaTiO_3$ bi-layer film shows excellent dielectric performance and energy storage characteristics, making this structure a promising candidate for applications in microelectronics as lead-free thin film ceramic capacitors.

Acknowledgments: The authors acknowledge the financial support of the Program for New Century Excellent Talents in University (State Education Ministry), Nano Projects of Soochow City (Grant No. ZXG201445), the Fundamental Research Funds of Shandong University (Grant No. 2015JC034, 2015YQ009). J.O. would also like to thank the "Qi-Lu Young Scholar Fund" of Shandong University and the support from the Material Measurement Laboratory of NIST, Gaithersburg, MD (USA).

Conflicts of Interest: The authors declare no conflict of interest.

Notes: For a ferroelectric, its *P-E* curve is close to *D-E* curve and the two notations (*P-E*, *D-E*) are often interchangeably used for one another. Rigorously, what is measured in a polarization-electric field test (*P-E* test) of a ferroelectric material is its *D-E* curve.

References

1. Wang, Y.; Zhou, X.; Chen, Q.; Chu, B.; Zhang, Q. Recent development of high energy density polymers for dielectric capacitors. *IEEE Trans. Dielectr. Electr. Insul.* **2010**, *17*, 1036–1042. [CrossRef]
2. Hao, X.; Wang, Y.; Yang, J.; An, S.; Xu, J. High energy-storage performance in $Pb_{0.91}La_{0.09}(Ti_{0.65}Zr_{0.35})$ O_3 relaxor ferroelectric thin films. *J. Appl. Phys.* **2012**, *112*, 114111. [CrossRef]
3. Hao, X.; Wang, Y.; Zhang, L.; Zhang, L.; An, S. Composition-dependent dielectric and energy-storage properties of (Pb,La)(Zr,Sn,Ti) O_3 antiferroelectric thick films. *Appl. Phys. Lett.* **2013**, *102*, 163903. [CrossRef]
4. Zhang, L.; Hao, X.; Zhang, L. Enhanced energy-storage performances of Bi_2O_3–Li_2O added $(1-x)(Na_{0.5}Bi_{0.5})TiO_3$–$xBaTiO_3$ thick films. *Ceram. Int.* **2014**, *40*, 8847–8851. [CrossRef]

5. Xie, Z.; Yue, Z.; Ruehl, G.; Peng, B.; Zhang, J.; Yu, Q.; Zhang, X.; Li, L. Bi($Ni_{1/2}Zr_{1/2}$)O_3-$PbTiO_3$ relaxor-ferroelectric films for piezoelectric energy harvesting and electrostatic storage. *Appl. Phys. Lett.* **2014**, *104*, 243902. [CrossRef]
6. Xie, Z.; Peng, B.; Meng, S.; Zhou, Y.; Yue, Z. High–Energy-Storage Density Capacitors of Bi ($Ni_{1/2}Ti_{1/2}$) O_3–$PbTiO_3$ Thin Films with Good Temperature Stability. *J. Am. Ceram. Soc.* **2013**, *96*, 2061–2064. [CrossRef]
7. Xie, Z.; Peng, B.; Zhang, J.; Zhang, X.; Yue, Z.; Li, L.; Trolier-McKinstry, S.E. Highly (100)-Oriented Bi($Ni_{1/2}Hf_{1/2}$)O_3-$PbTiO_3$Relaxor-Ferroelectric Films for Integrated Piezoelectric Energy Harvesting and Storage System. *J. Am. Ceram. Soc.* **2015**, *98*, 2968–2971. [CrossRef]
8. Xie, Z.; Yue, Z.; Peng, B.; Zhang, J.; Zhao, C.; Zhang, X.; Ruehl, G.; Li, L. Large enhancement of the recoverable energy storage density and piezoelectric response in relaxor-ferroelectric capacitors by utilizing the seeding layers engineering. *Appl. Phys. Lett.* **2015**, *106*, 202901. [CrossRef]
9. Xie, Z.; Peng, B.; Zhang, J.; Zhang, X.; Yue, Z.; Li, L. Effects of thermal anneal temperature on electrical properties and energy-storage density of Bi($Ni_{1/2}Ti_{1/2}$)O_3–$PbTiO_3$ thin films. *Ceram. Int.* **2015**, *41*, 206–212. [CrossRef]
10. Lee, B.D.; Lee, H.R.; Yoon, K.H.; Cho, Y.S. Microwave dielectric properties of magnesium calcium titanate thin films. *Ceram. Int.* **2005**, *31*, 143–146. [CrossRef]
11. Huang, C.L.; Chen, Y.B. Structure and electrical characteristics of RF magnetron sputtered $MgTiO_3$. *Surf. Coat. Technol.* **2006**, *200*, 3319–3325. [CrossRef]
12. Tkach, A.; Almeida, A.; Moreira, J.A.; Perez de la Cruz, J.; Romaguera-Barcelay, Y.; Vilarinho, P.M. Low-temperature dielectric response of $NaTaO_3$ ceramics and films. *Appl. Phys. Lett.* **2012**, *100*, 192909. [CrossRef]
13. Liu, G.Z.; Wang, C.; Wang, C.C.; Qiu, J.; He, M.; Xing, J.; Jin, K.J.; Lu, H.B.; Yang, G.Z. Effects of interfacial polarization on the dielectric properties of $BiFeO_3$ thin film capacitors. *Appl. Phys. Lett.* **2008**, *92*, 122903. [CrossRef]
14. Lee, S.J.; Kang, K.Y.; Kim, J.W.; Han, S.K.; Jeong, S.D. Low-Frequency Dielectric Properties of Sol-Gel Derived $BaTiO_3$ Thin Films. In Proceedings of the Materials Research Society, Nashville, TN, USA, 28 September–1 October 2011.
15. Yuan, M.; Zhang, W.; Wang, X.; Pan, W.; Wang, L.; Ouyang, J. In situ preparation of high dielectric constant, low-loss ferroelectric $BaTiO_3$ films on Si at 500 °C. *Appl. Surf. Sci.* **2013**, *270*, 319–323. [CrossRef]
16. Zhu, H.; Sun, X.; Kang, L.; Zhang, Y.; Yu, Z.; Ouyang, J.; Pan, W. Microstructural and electrical characteristics of epitaxial $BiFeO_3$ thick films sputtered at different Ar/O_2 flow ratios. *CrystEngComm* **2016**, *18*, 4604–4612. [CrossRef]
17. Gao, Y.; Yuan, M.; Sun, X.; Ouyang, J. In situ preparation of high quality $BaTiO_3$ dielectric films on Si at 350–500 °C. *J. Mater. Sci. Mater. Electron.* **2016**. [CrossRef]
18. Lee, C.C.; Wu, J.M. Effect of film thickness on interface and electric properties of $BiFeO_3$ thin films. *Appl. Surf. Sci.* **2007**, *253*, 7069–7073. [CrossRef]
19. Yan, F.; Zhu, T.J.; Lai, M.O.; Lu, L. Influence of oxygen pressure on the ferroelectric properties of $BiFeO_3$ thin films on $LaNiO_3$/Si substrates via laser ablation. *Appl. Phys. A* **2010**, *101*, 651–654. [CrossRef]
20. Dho, J.; Qi, X.; Kim, H.; MacManus-Driscoll, J.L.; Blamire, M.G. Large Electric Polarization and Exchange Bias in Multiferroic $BiFeO_3$. *Adv. Mater.* **2006**, *18*, 1445–1448. [CrossRef]
21. Zhu, H.; Liu, M.; Zhang, Y.; Yu, Z.; Ouyang, J.; Pan, W. Increasing energy storage capabilities of space-charge dominated ferroelectric thin films using interlayer coupling. *Acta Mater.* **2016**, *122*, 252–258. [CrossRef]
22. Hussain, S.; Hasanain, S.K.; Hassnain Jaffari, G.; Ismat Shah, S. Thickness dependent magnetic and ferroelectric properties of $LaNiO_3$ buffered $BiFeO_3$ thin films. *Curr. Appl. Phys.* **2015**, *15*, 194–200. [CrossRef]
23. Yuan, M.L. Medium Temperature Preparation of $BaTiO_3$ Thin Film Capacitors with High Breakdown Voltages and Large Electric Energy Densities. Master's Thesis, Shandong University, Jinan, China, 2014.
24. Zhang, W.; Gao, Y.; Kang, L.; Yuan, M.; Yang, Q.; Cheng, H.; Pan, W.; Ouyang, J. Space-charge dominated epitaxial $BaTiO_3$ heterostructures. *Acta Mater.* **2015**, *85*, 207–215. [CrossRef]
25. Tagantsev, A.K.; Landivar, M.; Colla, E.; Setter, N. Identification of passive layer in ferroelectric thin films from their switching parameters. *J. Appl. Phys.* **1995**, *78*, 2623. [CrossRef]
26. Roytburd, A.L.; Zhong, S.; Alpay, S.P. Dielectric anomaly due to electrostatic coupling in ferroelectric-paraelectric bilayers and multilayers. *Appl. Phys. Lett.* **2005**, *87*, 092902. [CrossRef]

27. Liu, Y.T.; Ku, C.S.; Chiu, S.J.; Lee, H.Y.; Chen, S.Y. Ultrathin oriented $BiFeO_3$ films from deposition of atomic layers with greatly improved leakage and ferroelectric properties. *ACS Appl. Mater. Interfaces* **2014**, *6*, 443–449. [CrossRef] [PubMed]
28. Simões, A.Z.; Riccardi, C.S.; Dos Santos, M.L.; Garcia, F.G.; Longo, E.; Varela, J.A. Effect of annealing atmosphere on phase formation and electrical characteristics of bismuth ferrite thin films. *Mater. Res. Bull.* **2009**, *44*, 1747–1752. [CrossRef]
29. Kawae, T.; Terauchi, Y.; Tsuda, H.; Kumeda, M.; Morimoto, A. Improved leakage and ferroelectric properties of Mn and Ti codoped $BiFeO_3$ thin films. *Appl. Phys. Lett.* **2009**, *94*, 112904. [CrossRef]
30. Wang, C.; Jin, K.J.; Xu, Z.T.; Wang, L.; Ge, C.; Lu, H.B.; Guo, H.Z.; He, M.; Yang, G.Z. Switchable diode effect and ferroelectric resistive switching in epitaxial $BiFeO_3$ thin films. *Appl. Phys. Lett.* **2011**, *98*, 192901. [CrossRef]
31. Sun, S.; Wang, Y.; Fuierer, P.A.; Tuttle, B.A. Annealing effects on the internal bias field in ferroelectric PZT thin films with self-polarization. *Integr. Ferroelectr.* **1999**, *23*, 25–43. [CrossRef]
32. Yan, F.; Zhu, T.J.; Lai, M.O.; Lu, L. Effect of bottom electrodes on nanoscale switching characteristics and piezoelectric response in polycrystalline $BiFeO_3$ thin films. *J. Appl. Phys.* **2011**, *110*, 084102. [CrossRef]